

# On the cosmological evolution of the FRII radio source population

Christian R. Kaiser<sup>1,2\*</sup> and Paul Alexander<sup>1</sup>

<sup>1</sup> MRAO, Cavendish Laboratory, Madingley Road, Cambridge, CB3 0HE, UK

<sup>2</sup> University of Oxford, Department of Physics, Nuclear Physics Laboratory, Keble Road, Oxford, OX1 3RH, UK

arXiv:astro-ph/9809269v2 21 Oct 1998

29 March 2021

## ABSTRACT

We present an analytical model for the cosmological evolution of the FRII source population. Based on an earlier model for the intrinsic radio luminosity - linear size evolution of these objects, we construct theoretical source samples. The source distributions in the radio power - linear size plane of these samples are then compared with that of an observed flux-limited sample. We find that the source parameters determining the radio luminosity of FRII objects can not be independent of each other. The best-fitting models predict the jet power to be correlated either with the life time of the source or with the shape of the density distribution of the source environment. The latter case is consistent with the observed tendency of the most luminous radio sources at high redshift to be located in richer and more extended environments than their low redshift counterparts. We also find evidence for a class of FRII sources distinctly different from the main population. These sources are extremely old and/or are located in very underdense environments. The luminosity function of FRII sources resulting from the model is in good agreement with previous results for high luminosity sources. The apparent luminosity evolution of the radio luminosity function is not reproduced because of the high flux limit of the used comparison sample. The cosmological evolution of the median linear size of FRII sources is found to be mild.

**Key words:** galaxies: active – galaxies: evolution – galaxies: jets – galaxies: luminosity function, mass function – cosmology: theory

## 1 INTRODUCTION

This is the third in a series of papers presenting an analytical model for the evolution of FRII radio sources. In Kaiser & Alexander (1997), hereafter KA, we developed a model for the general dynamics of these sources. The intrinsic evolution of the radio luminosity of a given radio source as a function of its linear size was investigated in Kaiser, Dennett-Thorpe & Alexander (1997), hereafter KDA. In this paper we use the model for the intrinsic radio luminosity-linear size evolution of FRII sources of KDA to constrain the cosmological evolution of these sources and their progenitors.

The radio power (P) - linear size (D) diagram was introduced by Shklovskii (1963) as a powerful tool to investigate the evolution of extragalactic radio sources. Baldwin (1982) pointed out that the P-D diagram is analogous to the Hertzsprung-Russel diagram for stars. However, there is a strong correlation between the radio luminosity and the redshift of sources in flux-limited samples. This Malmquist

bias implies that the source distribution in the P-D plane of such samples is a result of the intrinsic evolution of individual sources and the cosmological evolution of the source population as a whole. KDA point out that the scarcity of radio sources with linear sizes greater than roughly 1 Mpc can be partly explained by the steepening of the evolutionary tracks through the P-D diagram of FRII sources caused by the energy losses of the relativistic electrons in their cocoons due to inverse Compton scattering of the Cosmic Microwave Background Radiation (CMBR). Since the energy density of the CMBR increases with redshift, the cut-off in linear size above which only very few sources are found will put important constraints on the cosmological evolution of the radio source population.

It is not clear why AGN formation occurs and how jet activity in galaxies is subsequently triggered. It is therefore also unknown whether all massive galaxies in the universe go through a phase of jet activity as part of their evolution or whether only those galaxies involved in violent processes like galaxy mergers can become active.

For the purpose of the analysis presented in this paper we will simply assume that there is a population of pro-

\* email: c.kaiser1@physics.oxford.ac.uk

genitors of radio sources without specifying exactly what they are. The only property these progenitors must have, is that they become active with a certain probability at some cosmological epoch, as described by the ‘birth function’, and then turn into a radio source whose intrinsic luminosity evolution is determined by the properties of the jets and the environment the progenitors are located in. With this assumption there are then two possibilities how cosmic evolution in the number density of radio sources can occur. Either all progenitors existing at a given redshift become active at some point in their life time and the evolution reflects the number of progenitors created at or before this redshift; or the progenitors are created very early in the evolution of the universe, have very long life times and jet activity is triggered by a process not intrinsic to the progenitor. In this case any evolution in the number density of radio sources indicates that the probability for this process to occur is varying with redshift. For convenience we will use only the latter interpretation in the formulation of the models in the following sections. However, it should be born in mind that there is no way inherent in the model to decide which interpretation is the more likely.

Assuming a birth function and a set of distribution functions characteristic of the environments of the progenitors, it is possible with the aid of the model described by KDA to predict a P-D diagram which accounts for observational selection effects. To constrain the models the predicted P-D diagram is then compared directly with the observed distribution of sources. Knowledge of the selection effects, and hence the use of a complete observational sample is essential for a proper statistical comparison. The only published sample of extragalactic radio sources with the completeness required for this analysis is the sample of Laing *et al.* (1983), hereafter LRL. In the original form the authors showed that the LRL sample is 96% complete to a flux limit of 10 Jy at 178 MHz for sources with angular sizes less than 10'. Riley (1989) showed that the sample is complete even for extended sources down to the surface brightness limit of the 6C survey of 120 mJy per beam (Baldwin *et al.* 1985). The sample subtends a solid angle of roughly 4.1 sr and contains 173 radio sources of which 30 are of type FRI. The remaining 143 sources are either quasars (43 sources) or radio galaxies (100 sources) with FRII morphology. We will assume here that quasars and FRII radio galaxies form one class of objects distinguished only by a different viewing angle at which they are observed (e.g. Barthel 1989). The model used here for the calculation of the radio emission of FRII sources does not include the emission of the radio core. The low selection frequency of LRL ensures that relativistically beamed radio emission from the radio core of FRII sources does not contribute significantly to the overall flux. However, two sources in the sample, 3C 345 and 3C 454.3, may have been included in the sample only because of their boosted core emission. The changes to the statistical properties of the LRL sample introduced by excluding these two sources are negligible. The source distribution of the LRL sample in the P-D plane is shown in Figure 1.

Once the most likely birth function and distribution functions of the progenitor properties is found, it is straightforward to derive the luminosity function of FRII sources from the model. Peacock (1985) and Dunlop & Peacock (1990) have used a large data base of deep radio obser-

vations to determine the luminosity function of all radio galaxies and quasars. Their free modelling approach allows the shape of the luminosity function to be constrained but does not explain why it has this shape. We show that the model described here is in agreement with their results and allows some conclusions as to the origin of the form of the luminosity function.

The median linear size of luminous sources in the LRL sample appears to be shorter than that of low luminosity sources (see Figure 1). Because of the correlation between luminosity and redshift in flux-limited samples this effect can also be interpreted in terms of a decrease in median linear size,  $D_{med}$ , with redshift (e.g. Masson 1980 and Macklin 1982). If interpreted in this way, this effect can be modelled with a power law,  $D_{med} \propto (1+z)^{n_D}$ . Several groups have tried to determine  $n_D$  and find very different values. Oort *et al.* (1987), Singal (1988), Kapahi (1989) and Subrahmanian & Swarup (1990) find  $n_D \sim 3$  while Eales (1985) and Neeser *et al.* (1995) derive  $n_D \sim 1.3$ . Neeser *et al.* (1995) showed that the strong evolution found in some samples could be caused by a selection effect in which FRI sources are mistakenly included in samples of FRII sources leading to an overestimate of the median linear size at low redshift. However, the observation that the maximum and the median linear sizes of high redshift and therefore luminous sources are shorter than those of their lower redshift and less luminous counterparts must be explained by any model predicting the radio source distribution in the P-D plane.

In Section 2 we construct samples of radio sources predicted by various source distribution functions and compare their distribution in the P-D plane with that of the LRL sample. The luminosity function of FRII sources predicted by the best-fitting models is derived in Section 3. In Section 4 we investigate the cosmological evolution of the median linear size of FRII objects as predicted by our model. A discussion of the implications of the model for the cosmological evolution of the radio source progenitor population is presented in Section 5. Throughout this paper we are using Friedmann world models with  $\Lambda = 0$  and  $H_o = 50 \text{ km s}^{-1} \text{ Mpc}^{-1}$ .

## 2 THEORETICAL SOURCE DISTRIBUTION IN THE P-D PLANE

In this section we describe the construction of theoretical P-D diagrams and the method employed to compare them with the observed distribution of FRII sources in the P-D plane.

### 2.1 The source distribution function

The model presented in KA and KDA for the radio luminosity and linear size evolution of a given radio source depends on a variety of source and environment parameters. If the density distribution of the gaseous environment of the source,  $\rho_x$ , is approximated by a King (1972) profile,

$$\rho_x = \rho_o \left[ 1 + \left( \frac{r}{a_o} \right)^2 \right]^{-\frac{\beta}{2}}, \quad (1)$$

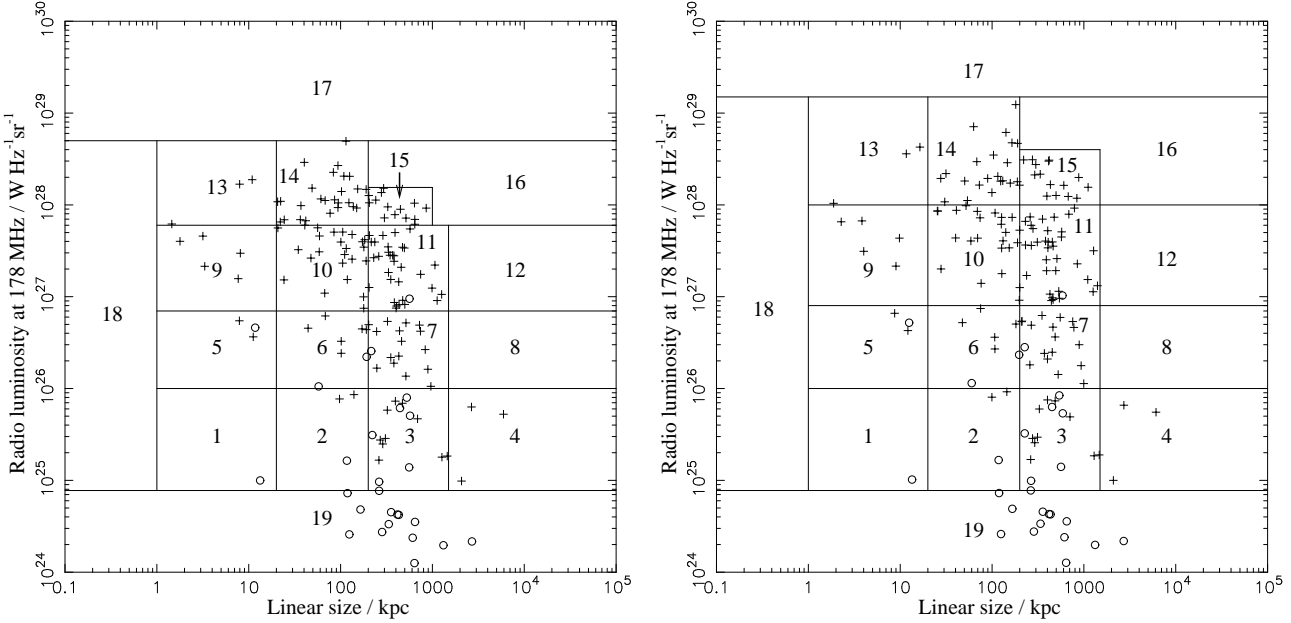


**Figure 1.** The source distribution of the LRL sample in the P-D plane. Left:  $\Omega_o = 1$ , right:  $\Omega_o = 0$ . Crosses: FRII-type radio galaxies and quasars, circles: FRI-type radio galaxies. The binning of the P-D plane used to compare model predictions to the LRL sample is shown.

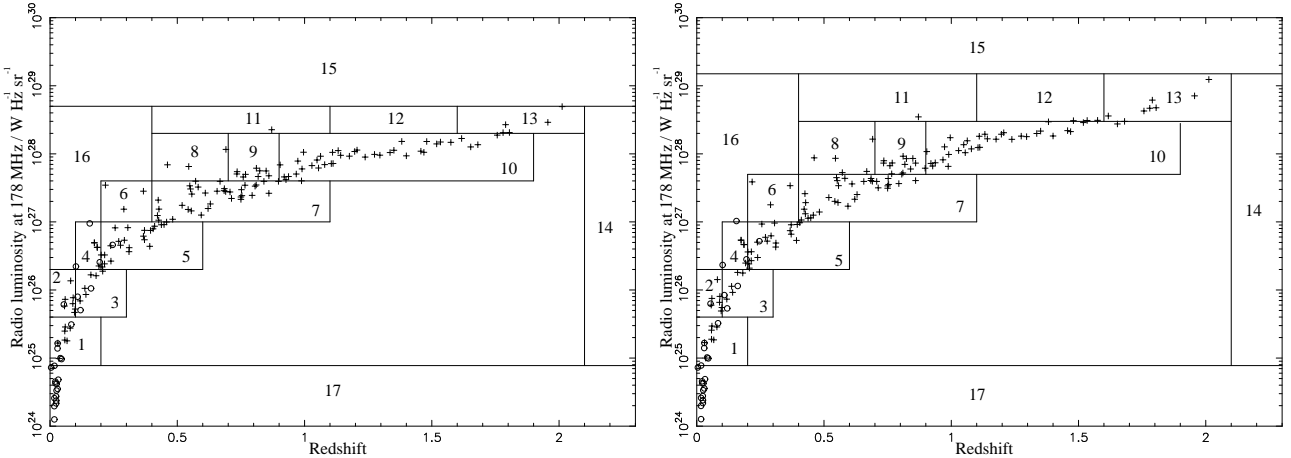


**Figure 2.** The source distribution of the LRL sample in the P-z plane. Left:  $\Omega_o = 1$ , right:  $\Omega_o = 0$ . Crosses: FRII-type radio galaxies and quasars, circles: FRI-type radio galaxies. The binning of the P-z plane used to compare model predictions to the LRL sample is shown.

where  $r$  is the radial distance from the centre of this distribution, these defining parameters are: The jet power,  $Q_o$ , the initial opening angle of the jet,  $\theta$ , the central density of the density distribution of the source environment,  $\rho_o$ , the core radius of this density distribution,  $a_o$ , and the exponent of the power law describing this distribution,  $\beta$ . Since it is not straightforward to measure  $\theta$  directly in observations, we will use the aspect ratio of the cocoon,  $R$ , i.e. the ratio of the length of the cocoon and its width, which is related to  $\theta$  by  $c_2/\theta^2 \approx 4R^2$  in the case of a ram-pressure confined cocoon, where  $c_2$  is a known constant (see KDA).

We assume that both, the energy density of the particles in the cocoon and that of the energy density of the magnetic field in the same region have relativistic equations of state which corresponds to case 1 in KDA. It was shown in

that paper that the specific choice of the equation of state in both cases does not significantly influence the shape of the resulting evolutionary tracks of a given source through the P-D diagram. Note also, that our choice implies equipartition between the energy density of the particles and that of the magnetic field in the whole cocoon. We also assume that the power law describing the energy spectrum of the relativistic electrons in the cocoon of all model sources extends from a Lorentz factor  $\gamma = 1$  to  $\gamma \rightarrow \infty$  and that the exponent of the power law is  $p = 2.25$ , implying mildly relativistic bulk velocities in the jets with a Lorentz factor of roughly 2 (Heavens & Drury 1988).

For a given choice of source and environmental parameters, together with the source age,  $t_i$ , the redshift of the source,  $z_p$ , and the viewing angle between the jet axis and

the line of sight,  $\alpha_v$ , the model developed in KDA yields a point on the P-D plane. In order to construct a complete theoretical P-D diagram one ideally needs to know the distribution function of each of the parameters mentioned above. Furthermore, the distribution functions of various parameters may not be independent, e.g. the sources with more powerful jets are also situated in higher density environments. For simplicity we assume initially that the distribution functions required in the model are independent. The number density of FRII sources in the universe as a function of jet and environmental parameters and of source age,  $t_l$ , can then be written as

$$\begin{aligned} d^6\rho = & \rho_{tot} N_1(\log_{10} Q_o) d(\log_{10} Q_o) N_2(R) dR \\ & \times N_3(\log_{10} \rho_o) d(\log_{10} \rho_o) N_4(a_o) da_o \\ & \times N_5(\beta) d\beta N_6(t_l) dt_l, \end{aligned} \quad (2)$$

where  $\rho_{tot}$  is the total number density of FRII sources in the universe and  $N_i$ , where  $i$  runs from 1 to 6, are the distribution functions of the jet and environmental parameters. All  $N_i$  are normalised to yield 1 when integrated over the entire range of the respective parameter.

In the chosen cosmology ( $\Lambda = 0$ ) the progenitors of radio sources of age  $t_l$  observed at redshift  $z_p$  became active at a cosmological epoch corresponding to

$$z_s = \left[ (z_p + 1)^{-\frac{3}{2}} - \frac{3H_o}{2} t_l \right]^{-\frac{2}{3}} - 1, \quad (3)$$

for  $\Omega_o = 1$  and

$$z_s = \frac{z_p + 1}{1 - H_o t_l (z_p + 1)} - 1, \quad (4)$$

for  $\Omega_o = 0$ . Let the probability for a progenitor to ‘switch on’ as a function of redshift, the ‘birth function’ of FRII sources, be  $N_7(z_s) dz_s$ . The distribution function of the ages of radio sources,  $t_l$ , observed at redshift  $z_p$  then is

$$\begin{aligned} N_6(t_l) dt_l = & N_7(z_s) \frac{dz_s}{dt_l} dt_l \\ = & N'_7(t_l, z_p) \frac{H_o}{\left[ (z_p + 1)^{-\frac{3}{2}} - \frac{3H_o}{2} t_l \right]^{\frac{5}{3}}} dt_l, \end{aligned} \quad (5)$$

for  $\Omega_o = 1$  and

$$N_6(t_l) dt_l = N'_7(t_l, z_p) H_o \left[ \frac{z_p + 1}{1 - H_o t_l (z_p + 1)} \right]^2 dt_l, \quad (6)$$

for  $\Omega_o = 0$ . If not stated otherwise we assume the remaining distribution functions  $N_i(A)$ , with  $i = 1 \dots 5$ , to be uniform;

$$N_i(A) dA = \frac{f(A_{max}, A_{min})}{A_{max} - A_{min}} dA, \quad (7)$$

where

$$f(A_{max}, A_{min}) = \begin{cases} 1 & ; A_{min} \leq A \leq A_{max} \\ 0 & ; A < A_{min} \text{ or } A_{max} < A \end{cases} \quad (8)$$

$N_6(t_l) dt_l$  in equations (5) and (6) is the fraction of all FRII sources in the universe with an age  $t_l$  at a cosmological epoch corresponding to redshift  $z_p$ . Of these only the sources located at coordinate distances between  $R_{o,r}(z_p)$  and  $R_{o,r}(z_p + dz_p)$  are observable. Assuming that the survey which we will use to compare our model predictions with

subtends a solid angle of  $\Omega$  and that the highest redshift at which progenitors become active is  $z_{max}$ , this fraction is found to be

$$\begin{aligned} \frac{dV(z_p)}{V(z_{max})} = & \frac{\Omega [R_{o,r}(z_p)]^2 d(R_{o,r})}{\Omega/3 [R_{o,r}(z_{max})]^3} \\ = & \frac{3}{2} \sqrt{\frac{(z_{max} + 1)^3}{(z_p + 1)^5}} \frac{(\sqrt{z_p + 1} - 1)^2}{(\sqrt{z_{max} + 1} - 1)^3} dz_p, \end{aligned} \quad (9)$$

in the case of  $\Omega_o = 1$  and

$$\begin{aligned} \frac{dV(z_p)}{V(z_{max})} = & \frac{3 (z_{max} + 1)^3}{z_{max}^3 (1 + \frac{1}{2}z_{max})^3} \\ \times & \frac{z_p^2 (1 + \frac{1}{2}z_p)^2 (1 + z_p + \frac{1}{2}z_p^2)}{(1 + z_p)^4} dz_p, \end{aligned} \quad (10)$$

for  $\Omega_o = 0$ .

From the jet and environmental properties it is possible to determine the linear size of a given radio source for any source age,  $t_l$ , and the observed linear size is determined by projecting onto the plane of the sky using a distribution function  $\sin \alpha_v d\alpha_v$  for viewing angles between  $\alpha_v$  and  $\alpha_v + d\alpha_v$ .

With these results the relative number of sources within the population of given jet and environmental parameters observed at redshift  $z_p$  and at a viewing angle  $\alpha_v$  are determined. Computationally, this is achieved by dividing the range over which a property  $A$  varies into small intervals  $\Delta A$ , which are then identified with the differentials  $dA$  in equation (2). The model for the radio emission of the cocoon described in KDA is then used to convert the chosen source properties into a linear size and a radio luminosity at the frequency in the rest-frame of the source,  $P_{\nu(z_p+1)}$ , corresponding to an observing frequency,  $\nu$ . The flux density which would be measured from the source is then

$$S_{\nu} = \frac{P_{\nu(z_p+1)}}{(R_{o,r})^2 (1 + z_p)}, \quad (11)$$

where  $R_{o,r}$  is the coordinate distance of the source. If this flux density is greater than the flux density limit of the observational sample the source is included in the model sample with the appropriate weight given by equation (2) and multiplied by  $dV(z_p)/V(z_{max}) \sin \alpha_v d\alpha_v$ .

Objects in flux-limited samples of observed radio sources span a large range in redshift. To obtain radio luminosities for these objects at the same frequency in the rest-frame of the individual sources it is usually assumed that the spectrum of radio galaxies is well represented by a power law,  $P'_{\nu} \propto \nu^{-\alpha}$ , where the spectral index,  $\alpha$ , is determined by measuring the flux of the radio galaxy at a second frequency. For the LRL sample this second frequency is 750 MHz. With this assumption equation (11) can be inverted to give

$$P'_{\nu} = S_{\nu} (R_{o,r})^2 (1 + z_p)^{1+\alpha}. \quad (12)$$

In order to mimic this procedure we calculate the radio luminosity of every source in the model samples at 178 MHz and 750 MHz from the model of KDA and derive the ‘observed’ spectral index,  $\alpha$ . With this and using equation (12) we then calculate the ‘observed’ radio luminosity,  $P'(\nu)$ , which is

then used to determine the location of the source on the P-D plane. Note, that  $P'_v$  is independent of the value of  $\Omega_o$  while the flux density calculated from equation (11) depends on the chosen cosmology. The sets of sources within the model samples are therefore different for different cosmologies.

Unless most of the radio emission from large sources is concentrated in the hot spots, it can be distributed over a large projected area on the sky. Even if the total flux of such sources is above the flux limit of a given sample, the sources may not be included in the sample because their surface brightness is below the detection limit of the telescope used to compile the survey from which the sample is drawn. In the model presented here we assume that the surface brightness of a given source is equal to its total luminosity divided by the projected area of sky covered by the cocoons. If the calculated surface brightness is below the surface brightness limit of the 6C sample, which was used to check the completeness of the LRL sample (Riley 1989), the source is not included in the model sample. Using this selection criterion we may omit some sources from our model samples which should be included because their radio emission is less smoothly distributed and their hot spots may be bright enough to be detected. However, in all the models presented here, the ‘number’ of sources excluded because of insufficient surface brightness was of order  $10^{-4}$  at most, which is negligible when compared to the number of sources,  $10^{-2}$  or higher, in the relevant bin which were included in the model sample.

## 2.2 Model parameters

The range over which the source parameters used in the model vary can in principle be deduced from observations, however, the constraints obtained in this way are incomplete and we will show later that there may also be considerable variation with redshift.

For the jet powers of FRII sources with redshifts below  $z = 1$  Rawlings & Saunders (1991) find  $10^{37} \text{ W} \leq Q^{rs} \leq 10^{40} \text{ W}$  from minimum energy arguments and  $\Omega_o = 0$ . For  $\Omega_o = 1$  these limiting values of  $Q^{rs}$  are somewhat lower but even for  $z = 1$  the correction factor necessary is less than 2. KDA point out that another correction due to an underestimate of the expansion work done by the cocoon by Rawlings & Saunders (1991) and to the potential presence of thermal material in the cocoon is necessary. Their equation (18) assumes that the rate at which energy is lost by the cocoon as expansion work as predicted by the model of KA is equal to half the jet power found by Rawlings & Saunders (1991). Because of the method used by Rawlings & Saunders (1991) it is more accurate to assume the rate at which energy is stored in the cocoon as predicted by KA to be equal to  $Q^{rs}/2$ . This implies that  $Q^{rs}$  is an overestimate of the jet power. When the additional energy of the thermal particles required by the model in KDA is also taken into account, we find that the correction to  $Q^{rs}$  is of order unity. We will therefore initially use  $Q_{o,min} = 10^{37} \text{ W}$  and  $Q_{o,max} = 10^{40} \text{ W}$ . A further discussion of this point is deferred to Section 3.

The source distribution of the LRL sample in the P-z plane (see Figure 2) implies that at every redshift there are more FRII sources of low radio luminosity in the universe

than very luminous objects. We therefore introduce an exponential distribution of jet powers,  $Q_o$ ;

$$N_1(\log_{10} Q_o) d(\log_{10} Q_o) = \frac{\lambda_q e^{-\lambda_q(\log_{10} Q_o - \log_{10} Q_{o,min})}}{1 - e^{-\lambda_q(\log_{10} Q_{o,max} - \log_{10} Q_{o,min})}} d(\log_{10} Q_o), \quad (13)$$

where  $\lambda_q$  varies from 0 to 10 in steps of 1.0. For  $\lambda_q = 0$  we use a uniform distribution of  $\log_{10} Q_o$  as described by equation (7).

For the aspect ratio of the cocoon,  $R$ , we use a uniform distribution with  $1.3 \leq R \leq 6.0$ , taken from Leahy & Williams (1984). The environments of FRII sources are either the IGM in clusters of galaxies or the atmospheres of the host galaxy itself in the case of small linear sizes or isolated objects. Canizares *et al.* (1987) find  $4 \cdot 10^{-23} \text{ kg/m}^3 \leq \rho_o \leq 5 \cdot 10^{-21} \text{ kg/m}^3$  for the central density of individual galaxies. The core radius of the density profile in these objects is  $0.01 \text{ kpc} \leq a_o \leq 2 \text{ kpc}$  with a median value  $\bar{a}_o \approx 1.0 \text{ kpc}$ . For clusters of galaxies Jones & Forman (1984) find  $7 \cdot 10^{-25} \text{ kg/m}^3 \leq \rho_o \leq 5 \cdot 10^{-23} \text{ kg/m}^3$  and  $30 \text{ kpc} \leq a_o \leq 1100 \text{ kpc}$  with  $\bar{a}_o \approx 260 \text{ kpc}$ . For simplicity we will calculate theoretical P-D diagrams for individual sources and sources in clusters separately and we will also assume that the core radius,  $a_o$ , for all model sources is equal to the respective median value  $\bar{a}_o$ . This implies  $N_4(a_o) da_o = \delta(a_o - \bar{a}_o) da_o$  in equation (2). For the central density we use a uniform distribution with  $\rho_{o,min} = 5 \cdot 10^{-23} \text{ kg/m}^3$  and  $\rho_{o,max} = 5 \cdot 10^{-21} \text{ kg/m}^3$  for isolated sources and  $\rho_{o,min} = 5 \cdot 10^{-25} \text{ kg/m}^3$  and  $\rho_{o,max} = 5 \cdot 10^{-23} \text{ kg/m}^3$  for sources in galaxy clusters.

In some of the following models we allow for cosmological evolution of the central density,  $\rho_o$ . If the properties of the environments of the progenitors only depend on redshift but not on any other source property, i.e. the jet power, they should all evolve in very similar ways. The central density,  $\rho_o$ , will in this case be proportional to the density of the gas filling the universe at the time when the progenitor and its environment decoupled from the Hubble flow. In this simplified picture we therefore expect that  $\rho_o \propto (1+z)^{n_d}$ , with  $n_d \leq 3$ .

The model for the radio emission of the cocoons of FRII sources described in KDA requires an external density distribution with  $\rho_x \propto r^{-\beta}$ . For distances from the centre of the density distribution,  $r$ , greater than a few core radii,  $a_o$ , the approximation  $\rho_x = \rho_o(r/a_o)^{-\beta}$  provides a good fit to equation (1). However, within the core radius this is not the case and sources in the centre of galaxy clusters will spend a considerable part of their life time in this region. We therefore split the external density profile into three different regimes:  $\rho_x = \rho_o$  for  $0 \leq r \leq a_o/2$ ,  $\rho_x = \rho_o/(2r/a_o)^{-\beta/2}$  for  $a_o/2 \leq r \leq 2a_o$  and  $\rho_x = \rho_o(r/a_o)^{-\beta}$  for  $r > 2a_o$ . During its life time a given radio source is changing from one density regime into the next when the linear sizes of its cocoons,  $L_j$ , reach  $a_o/2$  and  $2a_o$  respectively. Let the cocoons of a given radio source reach a linear size of  $a_o/2$  each at an age of  $t_l(L_j = a_o/2) = t_{l,0}(L_j = a_o/2)$ . During this time the external density profile is assumed to be  $\rho_x = \rho_o$ . If the source was located in a density regime with  $\rho_x = \rho_o(2r/a_o)^{-\beta/2}$  while expanding to this linear size, its age would be  $t_{l,\beta/2}(L_j = a_o/2) \neq t_{l,0}(L_j = a_o/2)$ . To

calculate the correct radio luminosity using the model presented in KDA once the cocoons of the source become larger than  $a_o/2$  and enter the second density regime, we have to use a fictitious source age  $t_{l,\beta/2}(L_j > a_o/2) = t_l(L_j > a_o/2) - t_{l,0}(L_j = a_o/2) + t_{l,\beta/2}(L_j = a_o/2)$  instead of the real source age  $t_l(L_j > a_o/2)$ . In other words, once the linear size of the cocoons of the radio source become larger than  $a_o/2$ , we treat the source for the calculation of its radio luminosity *as if* it had been located in an environment with  $\rho_x = \rho_o(2r/a_o)^{-\beta/2}$  for a time equal to the fictitious source age. Sources with cocoons larger than  $2a_o$  entering the third density regime are treated in an analogous way. The aspect ratio of the cocoon,  $R$ , is assumed to remain constant when the source changes from one regime to the next. We assume a uniform distribution of  $\beta$  between 1.0 and 2.0.

The viewing angle,  $\alpha_v$ , is distributed according to  $\sin \alpha_v d\alpha_v$  over the range 0 to  $\pi/2$  radians and for the source age we assume a maximum value of  $t_{l,max} = 10^9$  years which is the upper limit of observed spectral ages (Alexander & Leahy 1987). For sources reaching the maximum age we assume that the jet ceases to supply the cocoon with energy. The subsequent drop in radio luminosity occurs fast because of the adiabatic expansion of the cocoons. Therefore we assume that the radio luminosity of a source of age  $t_{l,max}$  drops to zero instantaneously.

The ratio of the number of progenitors becoming FRII sources with powerful jets to that of objects with weaker jets is given by equation (13) and is constant for all redshifts. The distribution of observed sources within the LRL sample in the P-z plane (see Figure 2) therefore suggests that the total number density of FRII sources in the universe is higher at higher redshift. To allow for this effect we introduce a birth function of the form  $N_7(z_s) dz_s \propto (z_s + 1)^n dz_s$ . The distribution function of the age of sources observed at redshift  $z_p$  then becomes

$$N'_7(t_l, z_p) = \frac{n+1}{(z_{max} + 1)^{n+1} - 1} \times \left[ (1 + z_p)^{-\frac{3}{2}} - \frac{3H_o}{2} t_l \right]^{-\frac{2}{3}n}, \quad (14)$$

for  $\Omega = 1$  and

$$N'_7(t_l, z_p) = \frac{n+1}{(z_{max} + 1)^{n+1} - 1} \times \left\{ \frac{z_p + 1}{[1 - H_o t_l (z_p + 1)]} \right\}^n, \quad (15)$$

for  $\Omega = 0$ . In both cases we investigate values of  $n$  between 0 and 10. Since there are no sources in the LRL sample beyond a redshift of roughly 2.1 we will use  $z_{max} = 5$  as the cut-off for the birth function. This ensures that even for  $\Omega = 0$  the first generation of radio sources which became active at a cosmological epoch corresponding to  $z_s = 5$  has reached the maximum source age at the cosmological epoch corresponding to  $z_p = 2.1$ .

### 2.3 $\chi^2$ -analysis

The comparison of the theoretical predictions for the distribution of radio sources in the P-D diagram with the LRL

sample is done by splitting the P-D plane into 19 bins as shown in Figure 1. The number of FRII-type sources for the LRL sample in each of the bins is given in the first column of Tables 1 and 2. Note, that the FRI-type objects in the LRL sample are not included in the binning process.

The way in which the P-D plane is binned and the number of bins will influence how well particular model predictions agree with the observed distribution for the LRL sample. Too many bins result in few sources in each occupied bin and it is then difficult within the  $\chi^2$  analysis to distinguish between occupied bins and those which are empty. As we have pointed out earlier, the maximum linear size of radio sources for each radio luminosity and the maximum radio luminosity within the whole sample are the strongest constraints on the cosmological evolution of the progenitor population. We have therefore chosen the bins in Figure 1 to delineate the source distribution of the LRL sample for large linear sizes and high radio luminosities without increasing significantly the number of bins.

For each set of model parameters for the progenitor population two ‘samples’ are calculated: one has external density profiles characteristic of isolated galaxies and the other density profiles appropriate to cluster environments. In all cases the flux density and surface brightness limits match those of the LRL sample. These ‘samples’ are then normalised to contain in total the same number of FRII-type objects as the LRL sample and binned in the way shown in Figure 1. The normalisation determines the total number density of FRII sources in the universe,  $\rho_{tot}$ , in equation (2).

The distribution of sources over the P-D diagram resulting from the model calculation is then compared with the one of the LRL sample using a  $\chi^2$  test. The probability that the source distribution of the LRL sample is a representation of a universe with the chosen source distribution function, equation (2), increases with decreasing  $\chi^2$ .

Since the redshifts of all objects in the LRL sample are known it is also possible to compare the model predictions with the distribution of observed sources in the P-z plane. Figure 2 shows the objects in LRL in this plane and the 17 bins used for the  $\chi^2$ -test here. The binning of the P-z plane is complicated by the Malmquist bias. Most sources in the LRL sample and the model samples are close to the line defined by the flux limit and it is difficult to find bins in this plane that will quantify the scatter about this line properly. Ideally one would like to use the two dimensional Kolmogorov-Smirnov test to compare the models with the observed data in the P-z plane. However, Peacock (1983) showed that the two dimensional KS test is unreliable if the two independent variables, in this case P and z, are strongly correlated. Since the main interest in this analysis is the P-D diagram we will compare only the best-fitting models with LRL on the P-z plane using the much simpler  $\chi^2$  method.

### 2.4 The cosmological evolution of the progenitor population

#### 2.4.1 Model A

In the first model considered, model A, all distribution functions of source and environmental parameters except that of the jet power,  $Q_o$ , are assumed to be uniform as described by the ‘top-hat’ function,  $f$ , given in equation (8). For the

bin	LRL	A		B		C		D		E		F		G	
		gal.	cl.												
1	0	0.73	0.27	0.66	0.16	0.54	0.19	0.61	0.21	0.61	0.21	0.34	0.13	0.35	0.15
2	2	6.78	6.75	5.95	3.31	4.81	4.05	6.06	4.67	5.05	4.20	3.26	2.77	3.51	3.45
3	10	16.46	16.72	13.24	7.22	10.59	8.64	11.22	9.86	8.96	8.14	7.23	6.52	8.09	8.09
4	3	2.41	0.32	1.44	0.17	0.73	0.11	0.33	0.08	0.60	0.09	0.46	0.03	0.35	0.04
5	2	0.67	0.19	1.11	0.41	1.00	0.46	1.28	0.44	1.24	0.58	0.90	0.47	1.35	0.62
6	6	5.06	6.35	6.72	7.85	5.55	8.74	8.24	8.20	7.23	9.79	7.32	8.91	9.46	10.30
7	16	12.64	19.06	12.26	15.95	9.17	16.46	11.49	14.29	11.04	15.61	12.65	14.89	13.81	16.32
8	0	4.38	1.21	1.98	0.49	0.99	0.28	0.45	0.13	1.0	0.18	0.32	0.00	0.28	0.00
9	5	1.11	0.32	1.60	0.91	2.65	1.38	2.89	1.34	4.11	2.35	3.38	2.07	3.76	2.12
10	23	9.55	9.22	11.25	14.52	18.47	21.71	22.37	20.50	25.64	27.25	28.03	31.20	26.05	26.60
11	32	23.95	29.86	22.02	28.89	34.00	39.41	33.44	35.57	35.87	32.39	34.80	34.43	32.08	26.19
12	0	11.03	5.03	3.28	0.92	2.10	0.49	0.73	0.25	1.33	0.19	0.12	0.00	0.25	0.00
13	3	2.74	0.54	2.88	2.04	5.04	1.82	4.24	2.14	5.87	3.88	4.16	2.07	4.52	3.35
14	27	19.45	12.46	19.79	23.75	21.51	18.54	21.48	22.01	20.86	25.23	25.94	24.46	22.47	28.78
15	14	12.39	14.57	11.79	14.09	24.83	20.64	18.30	23.30	12.80	12.91	13.55	13.65	16.32	17.03
16	0	13.71	20.24	22.57	17.74	0.76	0.09	0.17	0.06	0.05	0.02	0.53	1.37	0.12	0.00
17	0	0.00	0.00	4.58	4.84	0.00	0.00	0.00	0.00	0.00	0.00	0.00	0.00	0.00	0.00
18	0	0.01	0.00	0.12	0.01	0.25	0.01	0.18	0.01	0.20	0.02	0.01	0.00	0.25	0.03
19	0	0.00	0.00	0.00	0.00	0.00	0.00	0.00	0.00	0.00	0.00	0.00	0.00	0.00	0.00
$\chi^2$	...	78.1	190.8	67.3	105.6	29.7	100.2	34.3	135.0	21.5	108.1	21.5	299.4	27.0	238.1
$\chi^2_4$	...	78.3	171.3	66.3	58.2	23.0	26.5	12.8	24.9	12.0	11.4	7.7	17.1	6.9	12.7

**Table 1.** The number of sources in each P-D bin as defined in Figure 1 for the LRL sample and models A to G for  $\Omega_0 = 1$ . gal. and cl. indicate the use of the isolated galaxy and the cluster density profile respectively.  $\chi^2$  is the result of the  $\chi^2$ -test for the respective model and  $\chi^2_4$  is the result of the  $\chi^2$ -test when omitting bin 4.

bin	LRL	A		B		C		D		E		F		G	
		gal.	cl.												
1	0	0.70	0.15	0.69	0.17	0.60	0.19	0.53	0.21	0.61	0.18	0.39	0.21	0.37	0.16
2	2	6.23	3.88	5.98	3.47	5.17	3.89	5.35	4.55	5.13	3.42	3.73	4.78	3.72	3.27
3	10	13.01	9.60	11.25	7.77	9.77	8.59	10.17	10.05	9.16	6.88	8.41	11.08	8.34	7.62
4	3	1.14	0.18	0.73	0.18	0.64	0.11	0.27	0.08	0.54	0.13	0.54	0.04	0.39	0.05
5	2	0.77	0.15	1.36	0.42	1.33	0.40	1.26	0.39	1.38	0.56	1.03	0.55	1.62	0.87
6	5	6.09	5.05	7.86	8.30	7.75	7.84	7.65	7.54	7.81	10.02	8.55	10.90	10.37	13.01
7	17	13.84	15.09	13.55	18.27	13.51	16.24	12.07	14.93	12.41	18.24	14.40	17.39	15.37	19.96
8	0	3.25	0.98	1.35	0.62	1.34	0.31	0.52	0.17	1.04	0.37	0.36	0.00	0.31	0.01
9	5	1.50	0.37	2.36	1.02	3.06	1.22	3.03	1.33	3.88	2.42	3.17	2.00	4.23	2.87
10	23	13.92	11.25	15.88	17.15	20.78	19.54	23.03	21.14	24.11	28.52	28.08	29.15	26.72	30.97
11	36	33.08	37.13	28.69	36.69	37.56	38.94	38.97	40.38	34.38	35.64	34.77	28.30	30.14	27.69
12	0	11.84	7.30	2.97	1.45	3.10	0.82	1.38	0.46	1.74	0.45	0.16	0.00	0.27	0.00
13	3	1.88	0.51	3.70	1.54	3.49	1.70	2.61	1.41	5.25	3.16	3.08	2.30	4.79	3.22
14	22	14.55	13.01	19.87	18.34	16.50	18.69	16.58	17.07	20.98	21.51	22.58	23.95	22.48	23.50
15	15	19.08	35.33	22.97	23.97	18.18	24.55	19.49	23.34	14.36	11.49	13.76	12.35	13.65	9.81
16	0	2.10	3.07	3.72	3.75	0.05	0.02	0.03	0.01	0.01	0.01	0.00	0.00	0.00	0.00
17	0	0.00	0.00	0.00	0.00	0.00	0.00	0.00	0.00	0.00	0.00	0.00	0.00	0.00	0.00
18	0	0.01	0.00	0.15	0.00	0.16	0.01	0.12	0.00	0.20	0.01	0.01	0.00	0.29	0.03
19	0	0.00	0.00	0.00	0.00	0.00	0.00	0.00	0.00	0.00	0.00	0.00	0.00	0.00	0.00
$\chi^2$	...	47.1	180.4	32.1	80.9	22.1	100.4	39.5	139.6	21.2	75.9	18.3	227.0	25.6	205.9
$\chi^2_4$	...	44.6	138.3	25.4	38.3	13.6	28.5	12.6	27.5	10.2	14.4	7.1	18.1	8.1	17.6

**Table 2.** The number of sources in each P-D bin as defined in Figure 1 for the LRL sample and models A to G for  $\Omega_0 = 0$ . gal. and cl. indicate the use of the isolated galaxy and the cluster density profile respectively.  $\chi^2$  is the result of the  $\chi^2$ -test for the respective model and  $\chi^2_4$  is the result of the  $\chi^2$ -test when omitting bin 4.

jet power the exponential distribution of equation (13) is assumed. The birth function is assumed to be a power law of redshift and the distribution of source ages is therefore given by equations (14) and (15) respectively. The best-fitting model parameters for both, the isolated galaxy and the cluster density profile of the progenitor environment are given in Table 3 for  $\Omega_o = 1$  and Table 4 for  $\Omega_o = 0$ . The resulting relative source numbers in the P-D bins for the best-fitting model together with the value of the  $\chi^2$ -test for this model are given in Table 1 for  $\Omega_o = 1$  and Table 2 for  $\Omega_o = 0$ .

For model A we note that the number of sources in the low luminosity bins are comparable to the LRL sample but in all cases there are too many powerful, large sources (bins 12 and 16). This implies that the median hot spot advance speed in the powerful sources is too high for the assumed set of distribution functions. The slope of the birth functions, equations (14) and (15), is steep in all cases; the exponent  $n$  is in the range of 5 to 7. Although very luminous sources are therefore, in this model, located preferentially at a higher redshift than the less luminous ones, the increased energy losses of the relativistic electrons in the cocoon due to the higher energy density of the CMBR at high redshift do not sufficiently steepen the evolutionary tracks of the most powerful sources.

#### 2.4.2 Model B

The hot spot advance speed of a given source depends crucially on the density distribution of the material the source is expanding into. An increase in the median external density will therefore on average slow the linear expansion of the jets. The density of the progenitor environments at low redshift, whether they are individual galaxy or cluster profiles, are constrained by observations. For model A most of the objects which have linear sizes larger than those of sources in LRL are luminous and therefore preferentially located at high redshifts. This trend strongly suggests that the density of the environments the progenitors are located in, increases with redshift, and therefore we have considered models in which upper and the lower limit of the range of the central density,  $\rho_o$ , varies with redshift, according to

$$\begin{aligned} \rho_{o,min} &= \rho_{o,min}(z_p = 0) (z_p + 1)^{n_d} \\ \rho_{o,max} &= \rho_{o,max}(z_p = 0) (z_p + 1)^{n_d}. \end{aligned} \quad (16)$$

In these expressions  $\rho_{o,min}(z_p = 0) = 5 \cdot 10^{-23} \text{ kg/m}^3$  and  $\rho_{o,max}(z_p = 0) = 5 \cdot 10^{-21} \text{ kg/m}^3$  for galactic and  $\rho_{o,min}(z_p = 0) = 5 \cdot 10^{-25} \text{ kg/m}^3$  and  $\rho_{o,max}(z_p = 0) = 5 \cdot 10^{-23} \text{ kg/m}^3$  for cluster density profiles as before. The parameter  $n_d$  is investigated in the range 0 to 9. The best fit obtained for model B predicts a very strong evolution of  $\rho_o$  with redshift independent of the form of external density or  $\Omega_o$ . If the density of the progenitor environments is independent of other source parameters as we have assumed here, we expect  $n_d \leq 3$  (see Section 2.2). Model B is therefore unphysical since it requires  $n_d > 9$ .

#### 2.4.3 Models C and D

Although the exponential distribution of jet powers, equation (13), ensures that there are many more progenitors developing weak jets as compared to those producing strong jets, the results of model B suggest a persisting overestimate of the number of sources with very powerful jets in the model sample. We have therefore considered a variant of model B with a maximum jet power of  $\log_{10}(Q_{o,max}/W) = 39.4$  in the case of  $\Omega_o = 1$  and  $\log_{10}(Q_{o,max}/W) = 39.7$  for  $\Omega_o = 0$  instead of  $\log_{10}(Q_{o,max}/W) = 40$ . For the best-fitting model parameters the resulting model C includes almost no sources which are too luminous. Unless otherwise stated the following model samples are calculated with a maximum jet power of  $10^{39.4} \text{ W}$  for  $\Omega_o = 1$  and  $10^{39.7} \text{ W}$  for  $\Omega_o = 0$ .

For the determination of the best-fitting set of model parameters in model C bin 4 was excluded from the  $\chi^2$ -test since it alone contributes up to 76% of the total deviation of the model from the data of the LRL sample found with the  $\chi^2$ -test. The contribution of bin 4 is so large that it dominates the fitting procedure and any model for which the distribution of the LRL sample in the P-D plane may be a very good representation, could be rejected as a bad fit, if there is a strong deviation of LRL from the model sample in bin 4 alone. This suggests that some or all of the sources of the LRL sample found in bin 4 represent a class of objects distinct from the rest of the sample. These sources must be unusually old and/or located in very underdense environments. In the following we will exclude bin 4 from the  $\chi^2$ -test when determining the best-fitting model parameters.

Although model C represents an improvement over models A and B, particularly in the case of galactic density profiles and  $\Omega_o = 0$ , the predicted redshift evolution of the central density,  $\rho_o$ , is again steeper than the physical limit in all cases. Another possible mechanism which could reduce the linear size of powerful jets at high redshift is the predominance of flat density profiles for the environments of progenitors at high  $z$ . This is consistent with the scenario of the cosmological evolution of the environments of the progenitors outlined above since we expect that at early stages of the evolution of regions which have decoupled from the Hubble flow, the density gradient within these regions is small. In model D we therefore introduce an exponential distribution for  $\beta$  peaking at  $\beta = 1$  which steepens for increasing redshift;

$$\begin{aligned} N_5(\beta) d\beta &= \frac{\lambda_\beta e^{-\lambda_\beta(\beta - \beta_{min})}}{1 - e^{-\lambda_\beta(\beta_{max} - \beta_{min})}} d\beta \\ \lambda_\beta &= \lambda_{\beta,0} + (z_p + 1)^{n_\beta} - 1, \end{aligned} \quad (17)$$

where  $\lambda_{\beta,0}$  and  $n_\beta$  vary from 0 to 4 in steps of 1. Although model D improves the model fit significantly in the case of individual galaxy density profiles, the predicted evolution of the central density is still too steep with  $n_d = 9$ .

#### 2.4.4 Model E

For models A to D we have assumed that the maximum age,  $t_{max}$ , of all radio sources is  $10^9$  years. If  $t_{max}$  decreases with increasing redshift, we expect the median linear size of radio sources to be smaller at higher redshift. Because of the strong correlation of redshift and radio luminosity in

	A		B		C		D		E		F		G	
	gal.	cl.	gal.	cl.	gal.	cl.	gal.	cl.	gal.	cl.	gal.	cl.	gal.	cl.
$\lambda_q$	4	4	4	3	5	4	5	5	4	4	2	1	5	5
$n$	6	5	1	0	6	4	6	7	5	5	3	0	5	6
$n_d$	...	...	9	9	9	9	9	9	6	9	...	...	...	...
$\lambda_{\beta,0}$	...	...	...	...	...	...	4	1	...	...	...	...	...	...
$n_{\beta}$	...	...	...	...	...	...	3	3	...	...	...	...	...	...
$n_t$	...	...	...	...	...	...	...	...	1.0	1.0	...	...	...	...
$n_{t,q}$	...	...	...	...	...	...	...	...	...	...	0.5	0.6	...	...
$n_q$	...	...	...	...	...	...	...	...	...	...	...	...	2.0	2.0
$\chi^2_4$	78.1	171.3	66.3	58.2	23.0	26.5	12.8	24.9	12.0	11.4	7.7	17.1	6.9	12.7
$\sigma$	0%	0%	0%	0%	15%	7%	75%	10%	80%	83%	97%	45%	99%	75%
$-\log_{10}(\rho_{tot})$	0.61	1.87	3.92	5.31	0.90	2.88	1.02	2.42	1.51	2.17	2.98	5.18	1.89	1.71

**Table 3.** The best-fitting model parameters for  $\Omega_o = 1$ . To determine the best fit between a model and the source distribution of the LRL sample bin 4 in Figure 1 was omitted. The value of the  $\chi^2$ -test for this case and the significance of the fit,  $\sigma$ , are given for each model. The normalisation of the source distribution function, equation (2), is given as negative logarithm of  $\rho_{tot}$  in units of  $\text{Mpc}^{-3}$ . As before *gal.* and *cl.* indicate the use of the isolated galaxy and the cluster density profile respectively.

	A		B		C		D		E		F		G	
	gal.	cl.	gal.	cl.	gal.	cl.	gal.	cl.	gal.	cl.	gal.	cl.	gal.	cl.
$\lambda_q$	4	4	4	3	4	4	5	5	4	3	2	2	5	4
$n$	7	7	2	0	3	4	7	8	4	2	2	2	5	3
$n_d$	...	...	9	9	9	9	9	9	8	9	...	...	...	...
$\lambda_{\beta,0}$	...	...	...	...	...	...	3	3	...	...	...	...	...	...
$n_{\beta}$	...	...	...	...	...	...	4	4	...	...	...	...	...	...
$n_t$	...	...	...	...	...	...	...	...	1.0	1.5	...	...	...	...
$n_{t,q}$	...	...	...	...	...	...	...	...	...	...	0.5	0.6	...	...
$n_q$	...	...	...	...	...	...	...	...	...	...	...	...	2.0	2.0
$\chi^2_4$	44.6	138.3	25.4	38.3	13.6	28.5	12.6	27.5	10.2	14.4	7.1	18.1	8.1	17.6
$\sigma$	0%	0%	9%	0%	70%	4%	76%	5%	90%	64%	98%	38%	96%	42%
$-\log_{10}(\rho_{tot})$	2.36	3.19	4.98	6.51	4.60	4.76	2.79	2.66	4.10	4.06	5.09	5.50	3.93	5.44

**Table 4.** The best-fitting model parameters for  $\Omega_o = 0$ . To determine the best fit between a model and the source distribution of the LRL sample bin 4 in Figure 1 was omitted. The value of the  $\chi^2$ -test for this case and the significance of the fit,  $\sigma$ , are given for each model. The normalisation of the source distribution function, equation (2), is given as negative logarithm of  $\rho_{tot}$  in units of  $\text{Mpc}^{-3}$ . As before *gal.* and *cl.* indicate the use of the isolated galaxy and the cluster density profile respectively.

flux limited samples this may imply a decreasing median linear size with increasing luminosity. To investigate this we introduce

$$t_{max} = t_{max,0} (z_p + 1)^{-n_t} \quad (18)$$

in model E, where  $t_{max,0}$  is  $10^9$  years and  $n_t$  varies from 0.0 to 4.0 in steps of 0.5. Although the fit in model E is improved as compared to the previous models, the predicted evolution of the central density,  $\rho_o$ , is again very steep. The decrease in the maximum life time of sources at high redshift which feature preferentially powerful jets, alone is not sufficient to reduce the median linear size of these objects as required by the observations. Note that, for the assumption of cluster density profiles, model E of all model samples calculated here, provides the best fit in both cosmologies with the observed LRL sample.

#### 2.4.5 Models F and G

To make progress and obtain a model which fits the distribution of the LRL sample in the P-D plane without invoking an unphysical evolution of the density of the progenitor

environment, we relax the assumption that all jet and environment parameter are independent of each other.

The model of the evolution of the radio luminosity of powerful radio galaxies described by KDA assumes that the power of the jet,  $Q_o$ , is constant over the entire life time of the source. Together with the uniform maximum age for these objects assumed here, this implies that the total energy transported from the AGN to the large scale structure,  $E_{tot}$ , during  $t_{max}$  is linearly proportional to  $Q_o$ , which may not necessarily be the case in radio galaxies. If the powerful jets exhaust their energy supply faster than their weaker counterparts, e.g.  $t_{max} \propto Q_o^{-n_{t,q}}$ , than this linear dependence is replaced by  $E_{tot} \propto Q_o^{1-n_{t,q}}$  and we expect the median linear size of the powerful sources to decrease. For model F we take

$$t_{max} = t_{max,0} \left( \frac{Q_o}{Q_{o,min}} \right)^{-n_{t,q}}, \quad (19)$$

where  $n_{t,q}$  is varying from 0.0 to 0.9 in steps of 0.1. We also take the maximum jet power,  $Q_{o,max}$ , to be  $10^{39.7}$  W for  $\Omega_o = 1$  and  $10^{40}$  W for  $\Omega_o = 0$  which improves the fit at the highest luminosities (bins 14 and 15). For the assumption of individual galaxy density profiles the model fit improves

to more than 97% significance for both cosmologies and the model predicts  $E_{tot} \propto Q_o^{0.5}$ . For cluster density profiles the fit is far less good.

Rawlings & Saunders (1991) find that the power of the jet is roughly comparable to the Eddington luminosity of the black hole in the AGN powering the jet at  $z \sim 1$ . Kormendy & Richstone (1995) find a correlation of the mass of the central black hole and the mass of the bulge in nearby galaxies. Since we model the density profile of the progenitor environment with a power law (equation 1), the total mass of the progenitor is proportional to the central density of this distribution,  $\rho_o$ . This may imply that the power of the jet in radio galaxies depends on the mass and the density of gas in the progenitor object. In model G we therefore take

$$\begin{aligned} \rho_{o,min} &= \rho_{o,min}(z_p = 0) \left( \frac{Q_o}{Q_{o,min}} \right)^{n_q} \\ \rho_{o,max} &= \rho_{o,max}(z_p = 0) \left( \frac{Q_o}{Q_{o,min}} \right)^{n_q}, \end{aligned} \quad (20)$$

where  $\rho_{o,min}(z_p = 0) = 5 \cdot 10^{-23} \text{ kg/m}^3$  and  $\rho_{o,max}(z_p = 0) = 5 \cdot 10^{-21} \text{ kg/m}^3$  for galactic and  $\rho_{o,min}(z_p = 0) = 5 \cdot 10^{-25} \text{ kg/m}^3$  and  $\rho_{o,max}(z_p = 0) = 5 \cdot 10^{-23} \text{ kg/m}^3$  for cluster density profiles as before. The maximum age of all sources is assumed to be  $10^9$  years and the maximum jet power is set to  $10^{39.4} \text{ W}$  for  $\Omega_o = 1$  and  $10^{39.7} \text{ W}$  for  $\Omega_o = 0$  as before. The exponent  $n_q$  is varied from 0.0 to 4.5 in steps of 0.5. The significance of the fit for the assumption of galactic density profiles is comparable to that of model F, while for cluster density profiles the fit improves compared to the last model.

#### 2.4.6 Comparison of models

Models F and G together with the assumption of galactic density profiles for the environment of the progenitors represent the best fit with the source distribution of the LRL sample in the P-D plane in both cosmologies of all the model calculations presented here. For the assumption of cluster density profiles model E provides a better fit than either model F or G. However, the very steep evolution of the central density,  $\rho_o$ , with redshift predicted by model E is unphysical and we will therefore restrict attention in the following section to models F and G with the assumption of galactic density profiles for the environments of the progenitor objects. The fact that the best-fitting parameters for models F and G are very similar, if not completely identical, for the two cosmologies investigated is remarkable given the higher radio luminosity required of sources to be included in the model sample and the higher maximum jet power used in the case of  $\Omega_o = 0$ . The source with the highest redshift in the LRL sample, 3C9, is located at roughly  $z = 2.1$ . The derived linear size and radio luminosity for an observed source at  $z = 2.1$  with measured angular size and radio flux density are a factor 1.6 and 2.6 respectively greater for  $\Omega_o = 0$  than for  $\Omega_o = 1$ . The resulting difference in the source distribution of the LRL sample on the P-D plane can apparently be accounted for in model F and G simply by the inclusion of sources with higher jet power in the model sample for the case  $\Omega_o = 0$ , without changing the model parameters.

To determine which of the two models is in better agree-

ment with the LRL sample we now compare the source distribution of the model samples with the best-fitting model parameters as given in Tables 3 and 4 in the P-z plane with that of the LRL sample. The results of the  $\chi^2$ -test for the binning of the P-z plane as introduced in Figure 2 are summarised in Table 5. Here again we have omitted the three sources of the LRL sample in bin 4 of the binning of the P-D plane. Note here, that the low value for the maximum jet power used in models F and G implies effectively a maximum radio luminosity for sources in the model samples. Together with the flux limit this means that the agreement of the model samples with the LRL sample in the P-z plane will be poor at the highest redshifts and also for the highest luminosities. If we restrict attention to lower redshifts and lower radio luminosities by omitting bins 11, 12 and 13 from the  $\chi^2$ -test, we find good agreement between the model samples and LRL. See also the following section for further discussion of this point. In both cosmologies the agreement between model G and the LRL sample is better than that between model F and LRL.

### 3 THE FRII LUMINOSITY FUNCTION

Using the results found in the previous section for the source distribution function, equation (2), it is now possible to derive the luminosity function of FRII sources,  $\rho(P_\nu, z)$ . Following the definition of Peacock (1985),  $\rho(P_\nu, z)$  is the number of radio sources per comoving volume measured in  $\text{Mpc}^3$  and per unit interval of  $\log_{10}(P_\nu)$  with  $P_\nu$  measured in  $\text{W Hz}^{-1} \text{ sr}^{-1}$ . This luminosity function is identical to the source distribution function divided by  $\log_{10}(P_\nu)$  but it is a function of the radio luminosity,  $P_\nu$  at frequency  $\nu$  and redshift, instead of the source and environmental parameters. To be able to compare our results with those of Dunlop & Peacock (1990) we use their observing frequency 2.7 GHz and calculate the ‘observed’ spectral index between 2.7 GHz and 1.4 GHz. The luminosity function is then determined for 10 bins of equal width in  $\log_{10} P_{2.7}$  from 23.0 to 28.0 in the same way as the model samples in the previous section. Note, that we are now interested in all radio sources in the whole universe and not only in those which are observable to us. We therefore do not have to multiply equation (2) by equation (9) or (10) respectively.

Figures 3 and 4 show the resulting luminosity function for models F and G with the assumption of galactic density profiles in the environments of the progenitors. The flattening of the function for the lowest luminosities and the steepening at the high luminosity end are caused by the limits placed on the jet power,  $Q_o$ , and the density of the progenitor environment. Sources of lower luminosity than approximately  $P_{2.7} = 2 \cdot 10^{24} \text{ W Hz}^{-1} \text{ sr}^{-1}$  are likely to have low jet powers which makes their jets susceptible to turbulence. Since FRI sources are not included in the model, the space density of low luminosity sources predicted here is a lower limit.

Almost all of the sources in the LRL sample are close to the observational cut-off introduced by the flux limit of the sample (see Figure 2). The one source in LRL in bin 11, the quasar 3C196, and the most distant source in LRL, the quasar 3C9, in bin 13 are clearly peculiar exceptions to this observation since they are far too luminous for their respec-

bin	LRL	$\Omega_o = 1$				$\Omega_o = 0$			
		F		G		F		G	
		gal.	cl.	gal.	cl.	gal.	cl.	gal.	cl.
1	6	7.09	4.44	7.46	6.06	6	8.96	9.41	8.56
2	5	1.76	2.44	1.98	2.67	5	2.29	3.81	2.35
3	6	6.92	8.02	8.93	10.66	5	7.59	10.92	9.39
4	5	3.31	5.27	3.64	3.47	5	4.20	5.57	4.53
5	23	17.90	20.15	20.83	19.95	20	15.16	17.31	17.52
6	3	5.56	8.59	4.76	3.59	3	7.46	7.38	6.71
7	35	34.36	31.62	31.91	28.49	32	29.22	26.72	29.22
8	3	6.04	10.09	4.78	3.48	5	7.78	6.82	5.65
9	9	11.01	12.96	12.73	11.13	14	15.13	13.14	15.43
10	39	39.82	30.45	42.39	50.54	34	31.26	28.96	37.34
11	1	0.04	0.00	0.00	0.00	1	0.82	1.13	0.13
12	0	0.19	0.00	0.02	0.00	3	3.78	4.82	1.22
13	5	0.28	0.00	0.03	0.00	7	0.76	0.94	0.12
14	0	0.00	0.00	0.00	0.00	0	0.00	0.00	0.00
15	0	0.00	0.00	0.00	0.00	0	0.00	0.00	0.00
16	0	1.69	4.47	1.06	0.69	0	2.22	2.24	1.21
17	0	0.00	0.00	0.00	0.00	0	0.00	0.00	0.00
$\chi^2$	...	118.7	$\infty$	1186.8	$\infty$	...	64.7	52.5	400.2
$\chi^2_r$	...	13.4	21.23	10.6	10.6	...	13.3	12.6	10.2
$\sigma$	...	50%	10%	72%	72%	...	51%	56%	74%

**Table 5.** The number of sources in each P-z bin as defined in Figure 2 for the LRL sample and models F and G for  $\Omega_o = 1$  on the left and  $\Omega_o = 0$  on the right. gal. and cl. indicate the use of the isolated galaxy and the cluster density profile respectively.  $\chi^2$  is the result of the complete  $\chi^2$ -test for the respective model and  $\chi^2_r$  is the result of the restricted  $\chi^2$ -test which omits bins 11, 12 and 13.  $\sigma$  is the significance of the fit using the restricted  $\chi^2$ -test.

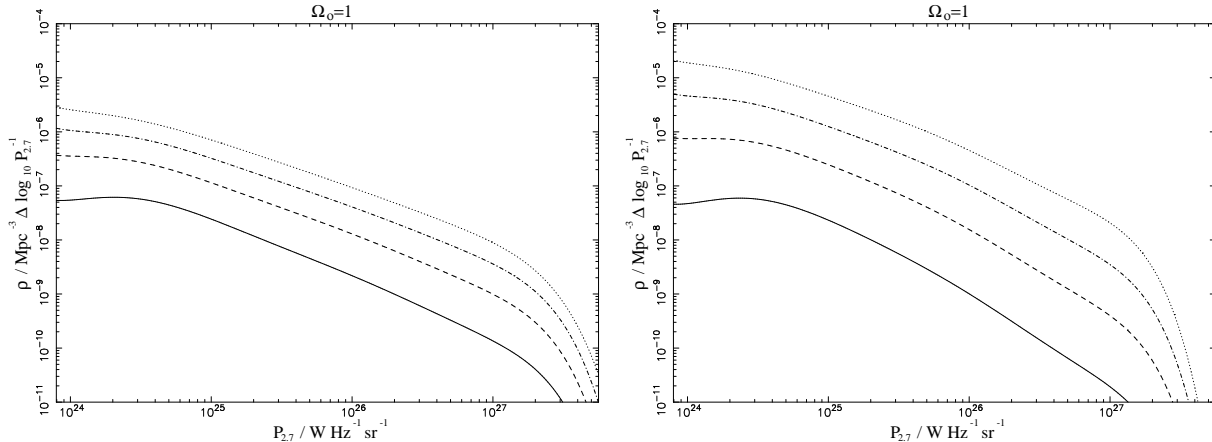


**Figure 3.** The FRII luminosity function for  $\Omega_o = 1$ . Left: model F, right: model G. Solid line:  $z=0$ , dashed:  $z=0.5$ , dot-dashed:  $z=1.0$  and dotted:  $z=1.5$ .

tive redshifts. The remaining sources in the LRL sample in bins 12 and 13 are difficult to reconcile with the very low relative source numbers in the model samples for models F and G, particularly in the case of  $\Omega_o = 1$ .

By introducing rather low maximum jet powers in the previous section it was possible to reduce the number of sources of high luminosity in the model samples but this also leads to a lack of sources in the model samples with luminosities and redshifts comparable to the highest luminosities and redshifts in the LRL sample. When included, the number of sources with the highest jet powers at high redshift is overpredicted by the model. This implies that, although the simple power law assumed for the birth function of radio

sources, equations (14) and (15), provides good model fits at low redshift it is not a good fit to the ‘true’ birth function at high redshift. The ‘true’ birth function must flatten or even turn over at high redshift to explain the comparatively small number of sources at these cosmological epochs. This is supported by a comparison of our results with those of Dunlop & Peacock (1990) presented in Figure 5. The flattening and the turn-over of the luminosity function predicted by their free-modelling approach occurs at redshifts comparable to those at which our model is overpredicting the number of sources with powerful jets when these are included in the model samples.

Dunlop & Peacock (1990) used an extensive data base

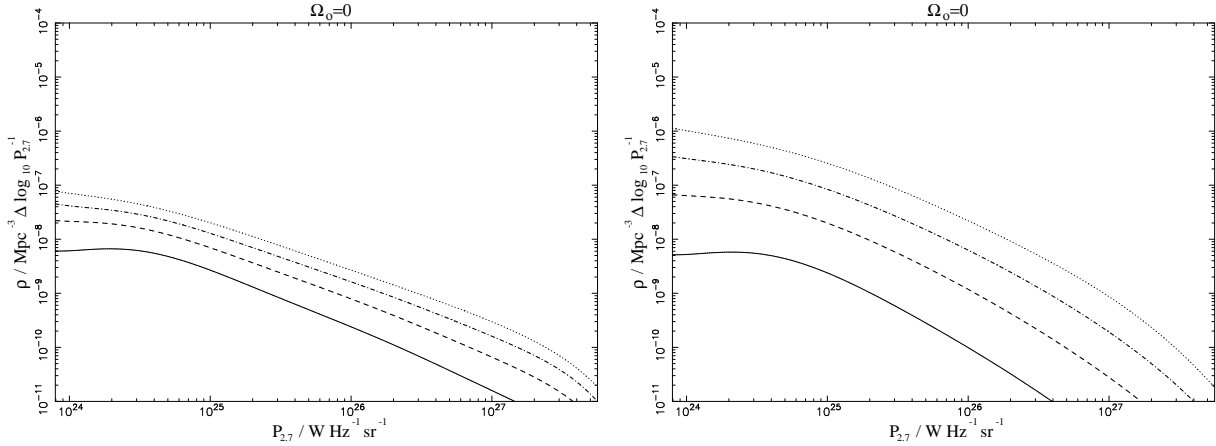


**Figure 4.** The FRII luminosity function for  $\Omega_0 = 0$ . Left: model F, right: model G. Solid line:  $z=0$ , dashed:  $z=0.5$ , dot-dashed:  $z=1.0$  and dotted:  $z=1.5$ .

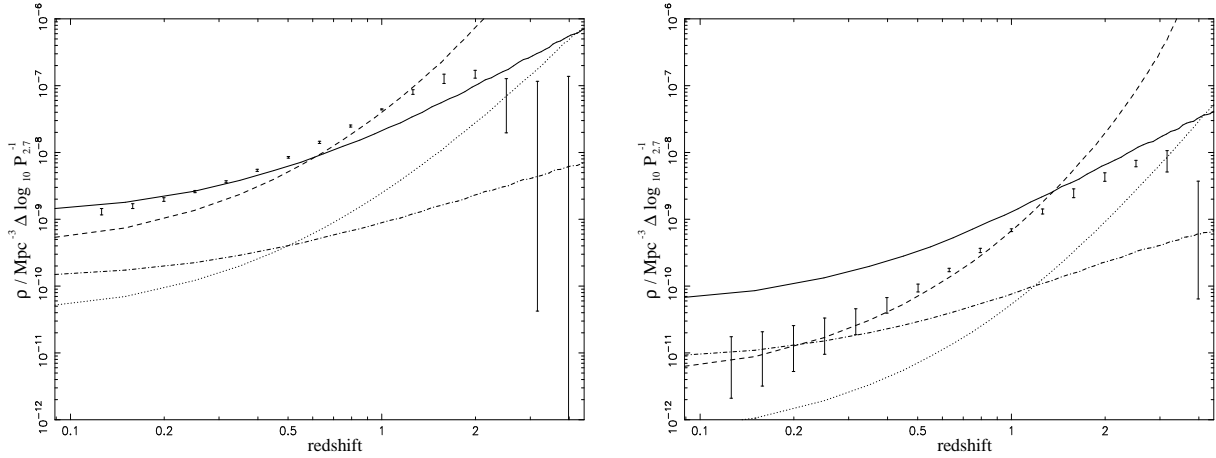


**Figure 5.** The FRII luminosity function as a function of redshift. Left:  $P_{2.7} = 10^{26} \text{ W Hz}^{-1} \text{ sr}^{-1}$ , right:  $P_{2.7} = 10^{27} \text{ W Hz}^{-1} \text{ sr}^{-1}$ . Solid line: model F for  $\Omega_0 = 1$ , dashed: model G for  $\Omega_0 = 1$ , dot-dashed: model F for  $\Omega_0 = 0$  and dotted: model G for  $\Omega_0 = 0$ . The error bars show the range of the luminosity function for  $\Omega_0 = 1$  as predicted by the free-modelling approach of Dunlop & Peacock (1990).

of observed sources with a flux limit at their observing frequency at 2.7 GHz of two orders of magnitude lower than that of LRL at 178 MHz as used in the previous section to constrain and normalise the model. The agreement between their results and the prediction of our models, particularly model G, is therefore remarkable.

The form of the cosmological evolution of the radio source population can be dominated either by space density evolution, or by luminosity evolution. The evolution of the FRII population as predicted by models F and G is dominated by the space density evolution of radio sources. This is a result of our assumption of independence of source and environment parameters. The ratio of sources with high jet power and those with low jet power is the same at each redshift and only the total number of radio sources is a function of  $z$ . Objects of similar jet power are also located in similar environments and have therefore similar radio luminosities regardless of their redshift. Exceptions to this rule are large sources which are already affected by the inverse Compton losses of the relativistic electrons in their cocoons. These sources have lower luminosities at higher redshifts because of the higher energy density of the CMBR at these epochs

and show therefore some luminosity evolution. In the case of pure density evolution or pure luminosity evolution the slope of the luminosity function will stay constant at all redshifts. Measuring the slope of the luminosity function predicted by our models between  $P_{2.7} = 10^{25} \text{ W Hz}^{-1} \text{ sr}^{-1}$  and  $P_{2.7} = 10^{27} \text{ W Hz}^{-1} \text{ sr}^{-1}$  in Figures 3 and 4 we find that this slope decreases from  $-1.2$  at  $z = 0$  to  $-0.9$  at  $z = 1.5$  in the case of model F. For model G the slope decreases from  $-1.5$  at  $z = 0.0$  to  $-1.2$  at  $z = 1.5$ . This slight flattening of the luminosity function with increasing redshift was also found by Dunlop & Peacock (1990) when they used a combined density-luminosity evolution model to fit their data.

Despite the luminosity evolution of large sources predicted by our models the overall evolution of the FRII population will be dominated by density evolution because of the set-up of our models. Fainter samples of FRII sources indicate that the evolution of the radio luminosity function for sources of lower luminosity is different from that of high luminosity sources (e.g. Dunlop & Peacock 1990). Some form of luminosity evolution therefore must take place. To model this behaviour of the radio luminosity function we would have to introduce a dependence of the birth function on the

jet power. This may also make it possible to avoid the low maximum jet power imposed on models F and G. However, this dependence would lead to an increase in the number of model parameters and since the LRL sample includes only the most luminous radio sources at any given redshift, the constraints on these additional parameters would be weak. We have therefore not investigated such models and our results presented here apply mostly to the high luminosity end of the radio luminosity function.

#### 4 LINEAR SIZE EVOLUTION

In order to determine the positions of a radio sources with given jet and environment parameters in the P-D plane we have already calculated the linear sizes of these sources. It is therefore straightforward to determine the median length of radio sources,  $D_{med}$ , as a function of redshift.

If fitted by a power law,  $D_{med} \propto (1+z)^{n_D}$ , we find  $n_D = -1.3$  for model F and  $n_D = -1.1$  for model G in both cosmologies. The model data is fitted well by a power law (correlation greater than 0.97) to  $z = 1.5$ . For higher redshifts the small number of sources in the model samples effectively prevents the determination of a meaningful value of  $D_{med}$ . Both values for  $n_D$  are within the error range of the value found by Neeser *et al.* (1995) from a statistical analysis of the sources in the LRL and the 6C sample (e.g. Eales 1985). There are no FRI-type objects in our model samples and our result can therefore be taken as a confirmation of the large selection effect pointed out by Neeser *et al.* (1995) in the derivation of the linear size evolution of radio sources.

When considering all radio sources in the universe we find  $n_D = -0.4$  for both models in both cosmologies. Also, the median linear size at  $z = 0$  is a factor 5 greater when all sources are taken into account as compared to the median linear size of the sources in the flux-limited model sample. This is consistent with larger sources being excluded from a flux limited sample because they are less luminous. The steeper linear size evolution in a flux-limited sample shows that this bias increases with increasing redshift.

#### 5 DISCUSSION

In the models considered in this paper we have assumed the birth function, i.e. the fraction of the radio source population becoming active as a function of cosmological epoch, to increase monotonically with redshift. Since the central black hole powering AGNs must form at some cosmological epoch, one expects the birth function to turn over at some redshift and our model will predict too many sources at higher redshifts. This effect is indeed present in our modelling and led us to introduce a lower maximum jet power since only sources with the highest jet powers and therefore highest radio luminosities are observable beyond the turn-over redshift. We find that our model fits the observational data well out to a redshift of about 1.5. The turn-over in the birth function, and therefore the peak in the radio luminosity function, must therefore occur beyond, but not far from,  $z = 1.5$ . This is consistent with the results of Dunlop & Peacock (1990).

The FRII objects in the LRL sample represent the

brightest radio sources in the universe at their respective cosmological epoch. They must therefore contain the most powerful AGNs and their cosmological evolution puts important constraints on the formation of structure in the universe. The median value of the jet power of sources in our model samples with the same flux limit as LRL as a function of redshift is well fitted by a power law and we find

$$Q_{o,med} = \begin{cases} 10^{38.0} (1+z)^{5.0} & \text{W ; model F} \\ 10^{37.6} (1+z)^{5.4} & \text{W ; model G} \end{cases}, \quad (21)$$

for  $\Omega_o = 1$  and

$$Q_{o,med} = \begin{cases} 10^{38.0} (1+z)^{5.9} & \text{W ; model F} \\ 10^{37.5} (1+z)^{6.2} & \text{W ; model G} \end{cases}, \quad (22)$$

for  $\Omega_o = 0$ . The boundaries of the range of central densities of the progenitor environment,  $\rho_o$ , are constant for model F while they are proportional to  $Q_o^2$  for model G. We therefore expect the median value of the central density as a function of redshift in the model samples to be constant in model F and to increase with redshift as determined by equations (21) and (22) in model G. However, the introduction of a flux limit may result in a deviation from this and indeed we find

$$\rho_{o,med} = \begin{cases} 10^{-21.0} (1+z)^{0.5} & \text{kg/m}^3 ; \text{ model F} \\ 10^{-19.8} (1+z)^{10.2} & \text{kg/m}^3 ; \text{ model G} \end{cases}, \quad (23)$$

for  $\Omega_o = 1$  and

$$\rho_{o,med} = \begin{cases} 10^{-21.0} (1+z)^{0.4} & \text{kg/m}^3 ; \text{ model F} \\ 10^{-19.9} (1+z)^{11.8} & \text{kg/m}^3 ; \text{ model G} \end{cases}, \quad (24)$$

in the case of  $\Omega_o = 0$ .

Equations (23) and (24) imply that the total mass of the progenitors of the most luminous radio galaxies in model G increase quickly with increasing redshift. Assuming that the gas in these objects is distributed according to equation (1) with  $\beta = 2$ , the total mass of the gas in the progenitor out to a radius  $R_x$  is given by

$$M_{tot} = \pi \rho_o a_o^3 \left( \frac{R_x}{a_o} - \arctan \frac{R_x}{a_o} \right). \quad (25)$$

For the observed galactic density profiles, which we have used in this analysis, Canizares *et al.* (1987) use  $R_x = 50a_o = 50$  kpc for the largest radius at which X-ray emission is detected in their objects. In both cosmologies, we derive total masses for the progenitors within this radius of order  $10^9 M_\odot$  for model F and of order  $10^{10} M_\odot$  for model G at  $z = 0$ . Out to redshift 1.5 this mass increases insignificantly in model F for both cosmologies. However, in model G we find  $M_{tot}$  at  $z = 1.5$  to be of order  $10^{14} M_\odot$  for  $\Omega_o = 1$  and of order  $10^{15} M_\odot$  for  $\Omega_o = 0$ . These derived mass concentrations for the radio source progenitors within a radius of 50 kpc are much higher than in any observed object. This may rule out model G.

Rawlings & Saunders (1991) showed that the radiated luminosity of AGNs is roughly equal to the power of the jets associated with them. Since at least the radiated energy of AGNs is provided by accretion of material onto a central black hole, this implies that the jet power can be written as

$$Q_o = \epsilon L_{Ed} = 1.25 \cdot 10^{31} \epsilon \frac{M_{BH}}{M_\odot} \text{W}, \quad (26)$$

where  $L_{Ed}$  is the Eddington luminosity of the central black

hole with mass  $M_{BH}$ .  $\epsilon$  is the fraction of the Eddington luminosity at which the AGN is supplying the jet with energy. In order for accretion onto the central black hole to be possible,  $\epsilon \leq 1$  is required. Theories of the formation of structure in the universe predict that the mass of the central black hole in any concentration of matter is proportional to the mass of the entire object,  $M_{tot}$  (e.g. Efstathiou & Rees 1988). This is confirmed by the masses of central black holes derived from observations of nearby galaxies (Kormendy & Richstone 1995). With equation (25) this implies  $Q_o \propto \epsilon \rho_o$ . Using equations (21), (22), (23), and (24) we find the following expressions for  $\epsilon$  of the brightest radio galaxies as a function of redshift.

$$\epsilon \propto \begin{cases} (1+z)^{4.5} & ; \Omega_o = 1, \text{ model F} \\ (1+z)^{-4.9} & ; \Omega_o = 1, \text{ model G} \\ (1+z)^{5.5} & ; \Omega_o = 0, \text{ model F} \\ (1+z)^{-5.6} & ; \Omega_o = 0, \text{ model G} \end{cases} \quad (27)$$

For increasing redshift  $\epsilon$  is increasing for model F while it is decreasing for model G. Rawlings & Saunders (1991) find the highest jet powers ( $\sim 10^{40}$  W) in sources at redshift 1. If  $\epsilon = 1$  in these sources, i.e. they are fuelling their jets at the Eddington limit, at  $z = 1.5$ , then the mass of their central black holes is of order  $10^9 M_{\odot}$ . In this case we find  $\epsilon$  at  $z = 0$  for model F to be equal to 0.016 for  $\Omega_o = 1$  and  $\epsilon = 0.006$  if  $\Omega_o = 0$ . For model G we find the rate at which energy is supplied to the jet to be highly super-Eddington at redshift 0 ( $\epsilon = 85$  for  $\Omega_o = 1$  and  $\epsilon = 162$  for  $\Omega_o = 0$ ). If  $\epsilon = 1$  in the brightest radio galaxies at  $z = 0$  instead of at  $z = 1.5$ , then model G predicts AGNs with black holes in their centre which are sub-Eddington for all redshifts. However, this implies that the mass of the central black hole in the most powerful sources at  $z = 1.5$  is equal to several  $10^{10}$  solar masses or higher. Although the existence of black holes with such large masses at high redshift can not be completely ruled out, the number of objects hosting such massive black holes is certainly very small (e.g. Efstathiou & Rees 1988). Note also, that in model F  $\epsilon \propto Q_o$  while in model G  $\epsilon \propto Q_o^{-1}$ . This implies that the energy conversion mechanism driving the jets in radio galaxies is more efficient in sources with high jet powers than in those with weaker jets in model F while in model G exactly the opposite is true.

In model F the life time of radio sources depends on the power of the jets. The median life time of the brightest radio sources is therefore also a function of redshift and we find  $t_{max} = 3.2 \cdot 10^7$  years for  $\Omega_o = 1$  and  $t_{max} = 2.2 \cdot 10^7$  years in the case of  $\Omega_o = 0$  at  $z = 1.5$ . This is consistent with observed spectral ages which usually do not exceed a few  $10^7$  years (Alexander & Leahy 1987). If the life time of the jets in radio galaxies is limited by the supply of fuel to their AGNs, then this implies that powerful jets are not only more efficient than weaker jets but also that they exhaust their fuel supply faster.

The very high mass concentrations in the environment of the progenitors and the need for black holes of extremely high mass in the centre of the AGNs driving the most powerful jets in model G, suggest that this model is unphysical. However, KA point out that the general dynamics of a radio source with given jet and environment parameters does not depend on  $\rho_o$  and  $a_o$  separately but only on the combination  $\rho_o a_o^{\beta}$  of these two quantities. The same is true for

the radio luminosity of the source derived from the model of KDA. The only difference between the evolutionary tracks through the P-D diagram of two sources with the same value of  $\rho_o a_o^{\beta}$  but different core radii and central densities is caused by the different fractions of their life time they spend in the three density regimes introduced in Section 2.2. In the following we will neglect the comparatively small effect these differences will have on the model parameters of model G and replace  $\rho_o$  by  $\rho_o a_o^{\beta}$ . With this we obtain  $\rho_o a_o^{\beta} \propto Q_o^2$  for model G. For the assumption that  $\epsilon = 1$  for all values of  $Q_o$  we then find  $a_o \propto Q_o^{1/(3-\beta)}$  and  $\rho_o \propto Q_o^{(6-3\beta)/(3-\beta)}$ . Using the redshift dependence of the jet power of the brightest radio galaxies, equations (21) and (22), and assuming  $\beta = 2$  we note that  $\rho_o$  is now a constant while  $a_o \propto (1+z)^{5.4}$  for  $\Omega_o = 1$  and  $a_o \propto (1+z)^{6.2}$  for  $\Omega_o = 0$ . Taking  $\rho_o = 5 \cdot 10^{-22}$  kg/m<sup>3</sup>, which is the median value of the distribution of  $\rho_o$  for the galactic density profiles, and  $a_o = 1$  kpc at  $z = 0$ , we find from equation (25)  $M_{tot} \sim 10^{12} M_{\odot}$  within a radius of 50 kpc at  $z = 1.5$  for both cosmologies. This is comparable to the mass contained within the same radius in M87 found from globular cluster dynamics (Cohen & Ryzhov 1997) and from thermal X-ray emission (Nulsen & Böhringer 1995). Note, however, that in the case discussed here, the core radius of the gas distribution of the environment,  $a_o$ , increases to 141 kpc for  $\Omega_o = 1$  and 293 kpc for  $\Omega_o = 0$  at redshift  $z = 1.5$ . Both values are much larger than those expected for the gas density profiles of individual galaxies and are more consistent with the gas distributions in galaxy clusters (Jones & Forman 1984). If  $\epsilon$  for the most luminous radio galaxies is not constant but decreasing with decreasing jet power, as is the case in model F,  $a_o$  will increase even more strongly with redshift while  $\rho_o$  may decrease with increasing redshift making the distribution of the gas in the environments of radio galaxies at high redshift even more similar to that in galaxy clusters.

Recently Best *et al.* (1998) showed that the host galaxies of the most luminous radio galaxies at  $z \sim 1$  are massive, highly evolved systems, presumably similar to the progenitors of the Brightest Cluster Galaxies (BCG). This is consistent with the tendency of the most luminous radio galaxies at high redshift to be located in richer environments than their low redshift counterparts (e.g. Hill & Lilly 1991). If we allow for the evolution of the core radius,  $a_o$ , of the density distribution in the environment of radio galaxies, our model G predicts a similar change in the environments of the most luminous radio galaxies from small, dense gas halos of individual galaxies at low redshift to more extended structures reminiscent of present day galaxy clusters at high redshift. This also explains the poor fit of our models with the LRL sample for the assumption of cluster-like density profiles in their environments at all redshifts.

The strong evolution of the radio luminosity of the most luminous radio galaxies in the universe with cosmic epoch (see Figure 2) is explained differently in models F and G. For the assumption that the mass of the central black hole is proportional to the total mass of the radio source progenitor, model F predicts that the mass of the central black hole powering the most luminous radio sources is essential constant with redshift. The strong decrease in radio luminosity is therefore caused by a less and less efficient energy conversion process which expresses itself in the decrease of  $\epsilon$  with cosmic time. We have shown that model G is consistent with

a constant value of  $\epsilon$  and the decrease of the radio luminosity is then in this model caused by a decrease of the mass of the central black hole in the centre of the most luminous radio galaxies. In the latter scenario some additional process is needed to explain why the most massive black holes do not produce jets with high jet powers at low redshift. The faster virialisation of the material in large objects like galaxy clusters as opposed to smaller groups could prevent gas from reaching the centre of potential radio source hosts within these rich environments at low redshift and thereby depriving the black holes in these objects of fuel (i.e. Best *et al.* 1998, Ellingson *et al.* 1991). This may explain why radio sources in clusters at low redshift are usually of type FRI which implies that their jets are comparatively weak.

## 6 CONCLUSIONS

Based on the models for the evolution of the linear size and radio luminosity of powerful extragalactic radio sources of type FRII presented in KA and KDA, we have investigated the distributions of various jet and environment parameters and their evolution with redshift within the FRII source population. The source distribution in the P-D plane predicted by our model is compared to that of the observed LRL sample. We find that our model predicts an unphysically strong evolution of the gas density in the source environment with redshift, if we assume that all jet and environment parameters are independent of each other. The best fit of the model to the data in the P-D plane is achieved by assuming that the life time of radio sources or the shape of the density distribution of their environments depends on the power of their jets.

Using this approach we find evidence that the giant sources in the LRL sample with linear sizes greater than 1.5 Mpc, DA240, 3C236 and 3C326, constitute a class of objects intrinsically different from the rest of the sample. They have to be extremely old and/or are located in extremely underdense environments.

The luminosity function of FRII sources derived from the models is in good agreement with the results of Dunlop & Peacock (1990). We find evidence for a flattening of the luminosity function beyond  $z = 1.5$ . The evolution of the luminosity function is dominated by density evolution but pure density evolution is ruled out because of the inverse Compton scattering losses of the CMBR off the relativistic electrons in the cocoons of radio sources. This result only applies to FRII sources with the highest radio luminosities at any given cosmological epoch which comprise the LRL sample. For lower luminosities the cosmological evolution of the FRII source population is probably different and the models presented here have to be modified to allow for such a behaviour of the radio luminosity function. Fainter complete samples of radio sources are also needed to better constrain the models at lower luminosities. The cosmological linear size evolution predicted by the models is consistent with the weak evolution derived by Neeser *et al.* (1995) from observations.

The best-fitting model predicting a correlation of the jet power with the source life time, model F, explains the decline of the radio luminosity of the most luminous radio galaxies with cosmic epoch in terms of a decrease in the efficiency

with which the jets are fuelled. The alternative model G requires cosmological evolution not only of the central density but also of the core radius of the density distribution of the material surrounding radio galaxies. This is consistent with the observed change in the environments of radio galaxies with cosmic epoch. In this model, the decline of the radio luminosity of the most luminous sources is caused by the decreasing mass of the central black holes powering the jets.

## ACKNOWLEDGEMENTS

We thank S. Rawlings, M. Lacy and the anonymous referee for helpful comments on the manuscript.

## REFERENCES

Alexander P., Leahy J. P., 1987, MNRAS, 225, 1  
 Baldwin J. E., Boysen R. C., Hales S. E. G., Jennings J. E., Waggett P. C., Warner P. J., Wilson D. M. A., 1985, MNRAS, 217, 717  
 Baldwin J. E., 1982, in Heeschen D. S., Wade C. M., eds, Extragalactic radio sources. Reidel, p. 21  
 Barthel P. D., 1989, ApJ, 336, 606  
 Best P. N., Longair M. S., Röttgering H. J. A., 1998, MNRAS, 295, 549  
 Canizares C. R., Fabbiano G., Trinchieri G., 1987, ApJ, 312, 503  
 Cohen J. G., Ryzhov A., 1997, ApJ, 486, 230  
 Dunlop J. S., Peacock J. A., 1990, MNRAS, 247, 19  
 Eales S. A., 1985, MNRAS, 217, 179  
 Efstathiou G., Rees M. J., 1988, MNRAS, 230, 5p  
 Ellingson E., Green R. F., Yee H. K. C., 1991, ApJ, 378, 476  
 Heavens A. F., O'C. Drury L., 1988, MNRAS, 235, 997  
 Hill G. J., Lilly S. J., 1991, ApJ, 367, 1  
 Jones C., Forman W., 1984, ApJ, 276, 38  
 Kaiser C. R., Alexander P., 1997, MNRAS, 286, 215  
 Kaiser C. R., Dennett-Thorpe J., Alexander P., 1997, MNRAS, 292, 723  
 Kapahi V. K., 1989, AJ, 97, 1  
 King I. R., 1972, ApJ, 174, L123  
 Kormendy J., Richstone D., 1995, ARA&A, 33, 581  
 Laing R. A., Riley J. M., Longair M. S., 1983, MNRAS, 204, 151  
 Leahy J. P., Williams A. G., 1984, MNRAS, 210, 929  
 Macklin J. T., 1982, MNRAS, 199, 1119  
 Masson C. R., 1980, ApJ, 242, 8  
 Neeser M. J., Eales S. A., Duncan-Green J., Leahy J. P., Rawlings S., 1995, ApJ, 451, 76  
 Nulsen P. E. J., Böhringer H., 1995, MNRAS, 274, 1093  
 Oort M. J. A., Katgert P., Steeman F. W. M., Windhorst R. A., 1987, A&A, 179, 41  
 Peacock J. A., 1983, MNRAS, 202, 615  
 Peacock J. A., 1985, MNRAS, 217, 601  
 Rawlings S., Saunders R., 1991, Nat., 349, 138  
 Riley J. M., 1989, MNRAS, 238, 1055  
 Shklovskii I. S., 1963, SvA, 6, 465  
 Singal A. K., 1988, MNRAS, 233, 87  
 Subrahmanyan K., Swarup G., 1990, MNRAS, 247, 237